Simulation and Project of a Reactor for Deposition of Transparent Oxide Conducting Films

Anna Beatriz Suppelsa[1], Fernando Fuzinatto Dall'Agnol[2], Angélica Denardi de Barros[1], Thebano Emílio de Almeida Santos[1]

asuppelsa@cti.gov.br, adbarros@cti.gov.br, fernando.dallagnol@ufsc.br, thebano.santos@cti.gov.br

[1]Núcleo de Microssistemas – NMS – CTI/MCTI Renato Archer – Campinas/SP
[2]Universidade Federal de Santa Catarina – Campus Blumenau

Abstract. *Atomic Layer Deposition (ALD) with vapor phase is one of the most important techniques applied in the production processes of thin films allowing precise control of their thickness and composition. The temperature on the substrate holder directly influences the deposition, whereas to obtain a balanced and uniform growth per cycle. Specific for transparent oxide conducting films these depositions, executed at temperatures between 300 °C and 400 °C due to the properties of the materials applied on devices nowadays, have to be extremely controlled. Therefore, this paper presents the modeling and simulation of an ALD reactor, verifying the gas dynamics and the temperature distribution achieved through the software COMSOL Multiphysics. The results obtained demonstrate the behavior of the substrate holder components influenced by environmental factors, enabling a suitable project of an ALD reactor [1], [2].*

Keywords: Atomic Layer Deposition, ALD, Atomic Layer Deposition Reactor, Ultra-Thin Films, TCO, Semiconductor Mixed Oxides, Simulation

1. Introduction

Atomic layer deposition (ALD) is a process derived from chemical vapor deposition (CVD), where the deposition process occurs through alternated pulses from the precursors at short intervals (between 0,2 s and 0,5 s), avoiding chemical reactions on their gas phase [3]. As in between those pulses, the gas in the chamber is completely removed, enabling the reaction to occur only on the substrate surface. An overdose of the precursor is administered on every pulse, saturating every reaction on its surface thoroughly. As a result, the reactions become self-limiting, allowing precise control of the film thickness [1], [2].

Early works analyses the atomic layer deposition process, [1], [3], [4], stating how the reaction and the depositions occur. Those researches also inform the applications of the technique, which ranges from nanotechnology coatings on particles and biotechnology to large-area coatings for photovoltaic applications [5].

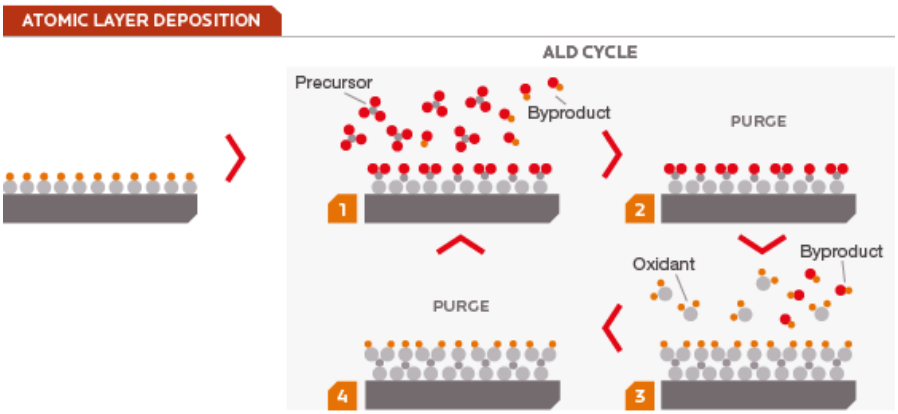

Figure 1 – Schematics of an ALD growth cycle [6]

Although the ALD technique allows precise control on the thickness of the thin-film produced, some problems regarding the substrate holder still need further research. Given that, the correct preparation of the substrate surface at the beginning of the process is essential and requires extreme attention to obtain a balanced and uniform growth per cycle. What occurs is that if the ALD reactor does not have a homogeneous heat distribution, the deposition will not be uniform.

According to *Johnson et al.* (2014), p. 236-246 [3], it became evident that *"the temperature range where the growth is saturated depends on the specific ALD process and is referred to as the 'ALD temperature window.' Temperatures outside of the window generally result in poor growth rates and non-ALD type deposition due to effects such as slow reaction kinetics or precursor condensation (at low temperature) and thermal decomposition or rapid desorption of the precursor (at high temperature). To benefit from the many advantages of ALD, it is desirable to operate within the designated ALD window for each deposition process."*

Therefore, it is essential to comprehend the behavior of the deposition by studying the temperature on the substrate holder, which allows the optimization of the deposition process of the TCO to occur effectively.

The objective of this research is to study the behavior of the temperature gradient in the reactor substrate holder, in addition to observing the main points of deformity and the physical phenomena that influence them. The main application of this work is, in addition to enabling a high-accuracy simulation of an ALD reactor, it also allows its subsequent optimization. As ALD reactors allow precise control of thin films, it is possible to obtain from it a more efficient deposition of transparent conductive oxides.

In this paper, we model an ALD reactor with the multipurpose software *COMSOL Multiphysics 5.2*. After creating its components, we define the physical phenomenon applied to the CAD geometry, and then, the study is computed. Finally, we compare the study results, discuss the implications of our work, and define the next steps to optimize the deposition technique.

2. Materials and Methods

2.1. 3D Model

This section focuses on the primary modeling of the tridimensional structure of the ALD reactor on the software *COMSOL Multiphysics 5.2*, using mainly the *CAD Import Module* and COMSOL's *Material Library*.

2.1.1. Geometry – Simulation Procedure 1

The reactor CAD final structure can be seen below in Figures 2 and 3. The structure was built based on the real model, measured with a pachymeter (analogical and digital) or ruler. The selected materials are from COMSOL's *Material Library*. Extra data indispensable for the simulation that was not already embedded in the material characteristics are taken from external references.

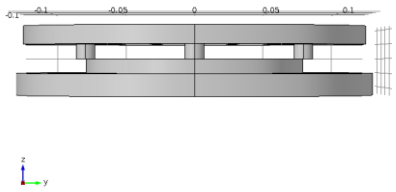

Figure 2 – Profile View of the 3D Model

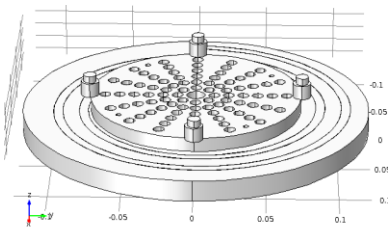

Figure 3 – Superior View of the 3D Model (Without Upper Plate)

Cast-Iron Plate

The first object modeled was the Cast-Iron plate, as seen in Figure 4. After defining the geometry *Parameters* on *Global Definitions*, the plate is created from a composition of cylinders.

Stainless Steel Plate

The next object modeled was the stainless-steel plate, which is the substrate holder (Figure 5); the material (*Stainless Steel*) was also chosen from COMSOL's built-in library. This stainless-steel plate is modeled in the same way as described in the previous geometry (Cast-Iron plate), with only the positioning and size of the holes being modified.

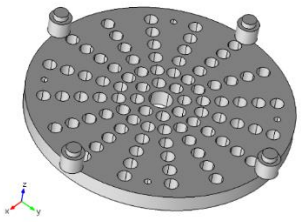

Figure 4 – Cast-Iron Plate 3D Model

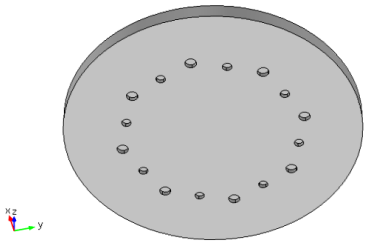

Figure 5 – Stainless Steel Plate 3D Model (Bottom View)

Chromel Resistance

The Chromel Resistance (material: *Chromel*, Figure 6), was the next object modeled. The geometry is a parameterized Archimedean spiral, which was made consulting a two-part tutorial [7], [8], that is also described on COMSOL's website [9].

White Pottery Clay Base

The white pottery clay base (Figure 7) is a support for the resistance, which was modeled by creating a cylinder (function *Build > Cylinder*). It has the same radius as the resistance, and its height is three times larger than the resistance. Furthermore, it is molded through the function *Difference* by deleting a copy of the chromel resistance.

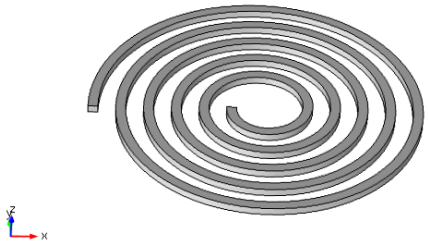

Figure 6 – Chromel Resistance 3D Model (Lateral View)

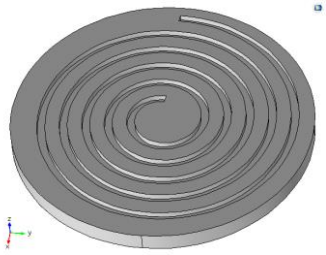

Figure 7 – White Pottery Clay Base (Upper View)

Form Assembly

Finally, the 3D geometry model is finalized by forming an assembly [10] and creating contact pairs (*Form Assembly > Create Pairs > Pair Type: Identity Pair*). The identity pairs are created automatically, but they must be correctly configured for the simulation to work correctly, for example, the source and destination boundaries need to be manually checked.

2.1.2.Geometry – Simulation Procedure 3

Simulation Procedure 3 also uses the 3D Model geometry, whereas the geometry has a few differences from the previous reactor model. Those differences are the addition of the air cylinder, and a slight alteration of the Cast-Iron plate supports.

Cast-Iron Plate Supports

When forming an assembly, there was a continuity error happening when trying to study the convection. So, to fix this error, the superior cylinder that was part of the support was disabled (Figure 8).

Air Cylinder

The Air Cylinder (Figure 9) is added to study both the convection and gas dynamics, such as laminar flow (velocity and pressure). The cylinder size was chosen arbitrarily so that it contained the reactor control volume.

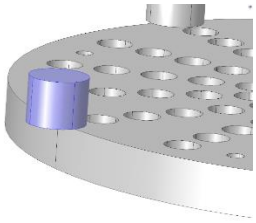

Figure 8 – New Cast-Iron Plate Supports 3D Model

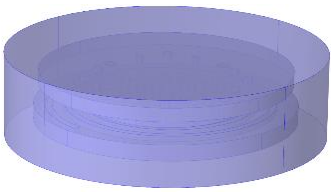

Figure 9 – Air Cylinder 3D Model (Lateral View)

2.2. Axial 2D-Symmetry Model

This section focuses on the implementation of the convection (Simulation Procedure 2) in an *Axial 2D-Symmetry* geometry model. This simulation runs in a significantly shorter time because the model has a less complex geometry, so it is easier to test and adapt that model to find better initial conditions that can be applied after on the 3D geometry.

2.2.1. Geometry – Simulation Procedure 2

The *Axial 2D-Symmetry* model (Figure 17) indicates that the geometry defined will rotate along the symmetry axis (defined as r = 0) after computing the study, forming a three-dimensional solid (Figure 10). This model simplifies the simulation since it requires less computational cost (and time) than the 3D model. Even though the structure of the reactor is mainly cylindrical, it is not entirely symmetrical, so parts of the geometry are not considered in this model. The geometry parts and respective materials are in Figure 11.

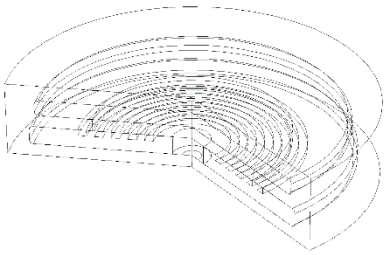

Figure 10 – 2D Model After Rotating Around Symmetry Axis

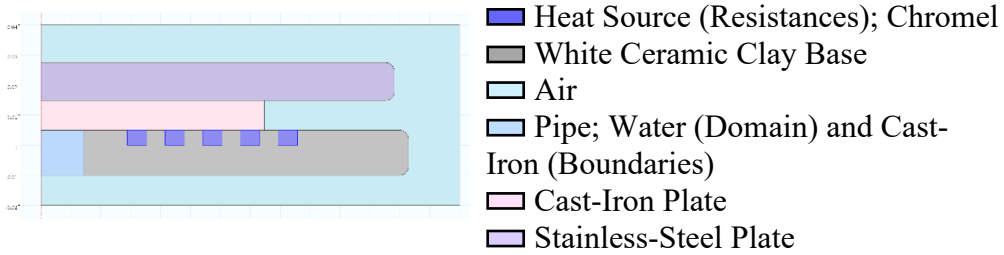

Figure 11 – 2D Model Components

The heat sources (resistances from the 3D Model) are rectangles that will compose concentric circles after rotating along the symmetry axis. Unlike the original model, which utilizes an electrical heat source in a spiral shape, this model's heat source dissipates heat on an average 6.5 W/cm^2, similar to a cooktop. The iron-cast 3D plate model contains internal holes and supports that sustain the stainless-steel plate, whereas

the 2D model does not have those components explicated; they are modeled using the *Thin Layer* pair boundary condition on the *Physics* section. The stainless-steel plate also does not contain holes due to the constraints of 2D-Axial Symmetry geometry.

2.3. Physics and Simulation Procedures

On COMSOL's interface, the physical phenomenon that will be analyzed must be chosen and defined through the *Physics* section (*Physics > Add Physics*). The selected *Physics* modules and the respective equations are described in Tables 1 and 2. The initial values are the same for all studies: T=293.15 K, and p = 1 atm.

<table>
<tr><th>Simulation / Module</th><th>Simulation 1</th><th>Simulation 2</th><th>Simulation 3</th></tr>
<tr><td rowspan="2">Heat Transfer</td><td rowspan="2">Heat Transfer in Solids (ht)</td><td>Heat Transfer in Solids</td><td>Heat Transfer in Solids</td></tr>
<tr><td>Heat Transfer in Fluids</td><td>Heat Transfer in Fluids</td></tr>
<tr><td>CFD Module</td><td>N/A</td><td>Laminar Flow (spf)</td><td>Laminar Flow (spf)</td></tr>
<tr><td>AC/DC</td><td>Electric Currents (ec)</td><td>N/A</td><td>Electric Currents (ec)</td></tr>
<tr><td rowspan="5">Multiphysics</td><td rowspan="2">Electromagnetic Heat Source 1 (emh1)</td><td rowspan="2">Non-Isothermal Flow 1 (nitfl)</td><td>Electromagnetic Heat Source 1 (emh1)</td></tr>
<tr><td>Boundary Electromagnetic Heat Source 1 (bemh1)</td></tr>
<tr><td>Boundary Electromagnetic Heat Source 1 (bemh1)</td><td>Temperature Coupling 1 (tc1)</td><td>Non-Isothermal Flow 1 (nitfl)</td></tr>
<tr><td rowspan="2">Temperature Coupling 1 (tc1)</td><td rowspan="2">Flow Coupling 1 (fc1)</td><td>Temperature Coupling 1 (tc1)</td></tr>
<tr><td>Flow Coupling 1 (fc1)</td></tr>
</table>

Table 1 – Physics modules on each simulation procedure

Module	Equations
Heat Transfer	**Simulation 1 and 3** $\rho C_p \frac{\partial T}{\partial t} + \rho C_p \mathbf{u} \cdot \nabla T + \nabla \cdot \mathbf{q} = Q + Q_{ted}$ [11], $\mathbf{q} = -k\nabla T$ [11] **Simulation 2** $\rho C_p \frac{\partial T}{\partial t} + \rho C_p \mathbf{u} \cdot \nabla T + \nabla \cdot \mathbf{q} = Q$ [11], $\mathbf{q} = -k\nabla T$ [11] $-\mathbf{n}_d \cdot \mathbf{q}_d = -\frac{1}{2} d_s \rho_s C_{ps} \frac{\partial T_{src}}{\partial t} - \frac{(T_{dst} - T_{src})}{R_s} + \frac{1}{2} d_s Q_s$ [11]; (*Thin Layer*)

CFD Module	**Simulation 1** N/A **Simulation 2** $\rho\frac{\partial \mathbf{u}}{\partial t}+\rho(\mathbf{u}\cdot\nabla)\mathbf{u}=$ [15], $\nabla\cdot\left[-p\mathbf{I}+\mu\left(\nabla\mathbf{u}+(\nabla\mathbf{u})^{T}\right)-\frac{2}{3}\mu(\nabla\cdot\mathbf{u})\mathbf{I}\right]+\mathbf{F}$ [15], $\frac{\partial \rho}{\partial t}+\nabla\cdot(\rho\mathbf{u})=0$ [15], $\left[-p\mathbf{I}+\mu\left(\nabla\mathbf{u}+(\nabla\mathbf{u})^{T}\right)-\frac{2}{3}\mu(\nabla\cdot\mathbf{u})\mathbf{I}\right]\mathbf{n}=\underset{\cdots}{-f_0}\mathbf{n}$ [15]; (*Open Boundary*), $\nabla\cdot\left[-p\mathbf{I}+\mu\left(\nabla\mathbf{u}+(\nabla\mathbf{u})^{T}\right)-\frac{2}{3}\mu(\nabla\cdot\mathbf{u})\mathbf{I}\right]+\underset{\cdots}{\mathbf{F}}$ [15]; (*Volume Force*) **Simulation 3** $-\mathbf{n}\cdot\mathbf{q}=\underset{\cdots}{q_0}$ [15], $q_0=h(T_{ext}-T)$ [15], $h=\frac{k}{H}\left(\frac{4}{3}\left(\frac{7Ra_H Pr}{5(20+21Pr)}\right)^{1/4}+\frac{4(272+315Pr)H}{35(64+63Pr)D}\right)$ [15]; (external) or $h=\frac{k}{H}\frac{Ra_D}{128}$ [15]; (internal)
AC/DC	**Simulation 1 and 3** V_0 = 50 V, $\nabla\cdot\mathbf{J}=Q_{j,v}$ [12], $\mathbf{J}=\sigma\mathbf{E}+\frac{\partial \mathbf{D}}{\partial t}+\mathbf{J}_e$ [12], $\mathbf{E}=-\nabla V$ [12]
Multiphysics	**Simulation 1 and 3** $\rho C_p\frac{\partial T}{\partial t}+\rho C_p\mathbf{u}\cdot\nabla T=\nabla\cdot(k\nabla T)+\underset{\cdots}{Q_e}$ [14]

Table 2 – Equations

All the studies are *Time-Dependent*, the intervals, steps, and computation time for each simulation procedure are in Table 3. Specifically, in Simulation Procedure 3, the study's *Methods and terminations* were altered on *Segregated Step 2* so that the Jacobian update happens "*on every iteration*": this configuration is essential for the convergence of the study.

Study	**Simulation 1**	**Simulation 2**	**Simulation 3**
Interval	0 to 20 minutes	0 to 60 seconds	0 to 70 seconds
Steps	4 minutes	1 second	1 second
Computation Time	2h 07min 22s	40 min 59 s	46 min 26 s

Table 3 – Study Configurations

I. Simulation Procedure 1

The first study in this section (Simulation Procedure 1) will determine and analyze its overall thermic distribution in the solid via conduction and radiation emissivity. This simulation couples the modules *Heat Transfer* and *AC/DC Module*. The convection is studied in the next section (Simulation Procedures 2 and 3), adding another component to the geometry, representing air.

It is important to note that the ALD reactor, that this simulation is based on, works with a PID Controller, so the voltage is not constant over time [13]. In this simulation, we are working with a constant voltage, to simplify the model and use less computational memory initially. Thus, several studies were computed by analyzing voltages from 20 V

to 110 V. After comparing those studies results - in the same time interval -, the most accurate voltage to reach the final temperatures of interest would be 50 V.

II. Simulation Procedure 2

This simulation procedure is studied within the Axial 2D-Symmetry Model. The modules from *COMSOL Multiphysics* used are the *Heat Transfer Module* and *CFD Module*.

The conjugated heat transfer couples both heat transfer in solids and fluids. Two *Thin Layer* boundary pairs are defined (between the cast ion plate and stainless steels, and between the heat sources and the Cast-Iron plate), indicating different heat conductions (same as how air would behave) between the boundaries. An *Open Boundary* (external boundaries from the air rectangle), *Heat Flux* (convection), and *Diffuse Surface* (indicating radiation on the external reactor boundaries) are defined. At last, the *Pair Boundary Heat Source* is defined on every boundary in contact with the resistances (*General Source*: 6.5 [W/cm^2]).

The *Laminar Flow Physics* is only selected on the domains that contain fluids; in this case, the air cylinder (containing air) and the tubulation (containing water). The study is an *Incompressive Flow*; the fluid properties are taken from the material, an *Open Boundary* is also defined (same as the heat transfer module), and a *Volume Force* is defined (r = 0; z = 10[N/m^3]*(T[1/K]-293.15) indicating the presence of gravity.

III. Simulation Procedure 3

Based on Simulation Procedure 2, the convection was implemented on the 3D Model, by adding *Heat Flux* (*Physics > Heat Transfer*) [16]. The modules from *COMSOL Multiphysics* used were also the *Heat Transfer Module* and *CFD Module*.

The configurations applied to the domains and boundaries are the same as Simulation Procedure 2, differentiating only on the Heat Source, which is the same as Simulation Procedure 1 (with AC/DC implemented).

3. Results and Discussions

3.1. Results – Simulation 1

After computing the first study (Simulation 1), the post-processed data (plots, graphs, and tables are made and analyzed [17].

I. Resistance Electric Potential

The applied electric tension (50 V) on the resistance boundary is constant; therefore, as expected, the potential in the chromel resistance domain remains the same during the study (Plot 1).

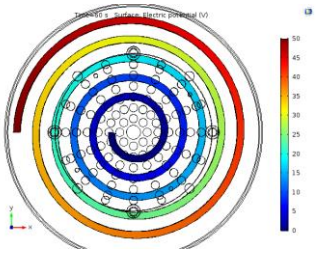

Plot 1 – 3D Plot – Resistance – Electric Potential (Volts)

II. Heating Curve and Heat Distribution (3D) - Temperature (ºC) x Time (s)

In Plot 2, four *Domain Probes* were created to analyze each object's heating curve individually. As expected, the highest temperatures are for the resistance, cast-iron plate, and stainless-steel plate, respectively. The heat distribution for t = 60s (Plot 3 and 4) shows that the temperature gradient is not uniform, with discrepancies on the middle of the cast-iron plate. These plots are also available on YouTube, in animation format [18], [19].

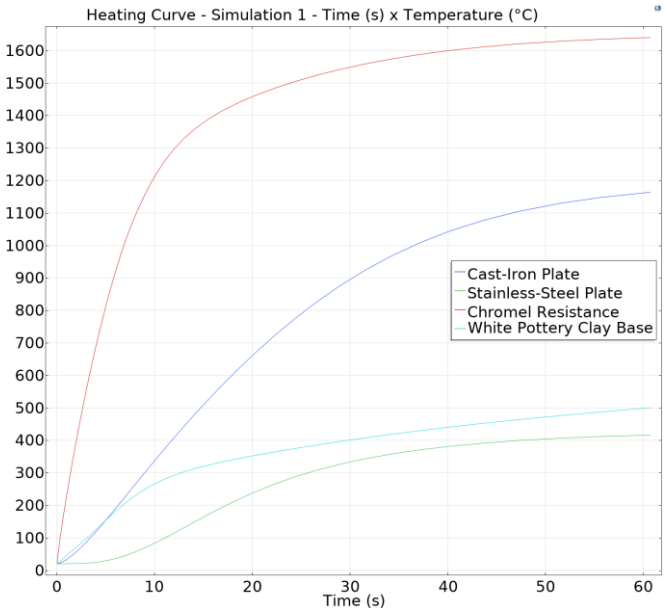

Plot 2 – Simulation 1 - Heating Curve – Temperature (ºC) x Time (s)

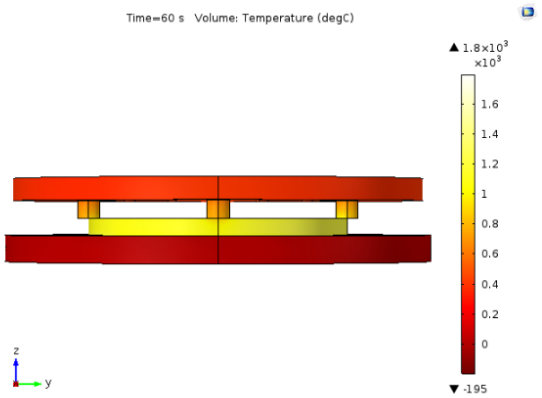

Plot 3 – 3D Plot – Heat Distribution (t = 60s); (Lateral View)

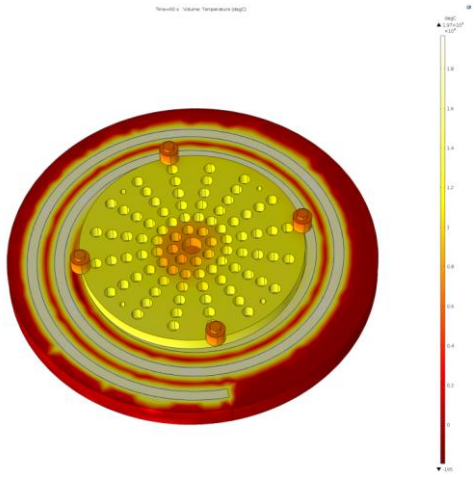

Plot 4 – 3D Plot – Heat Distribution (t = 60s); (Upper View, Stainless Steel Plate Hidden)

3.2. Results – Simulation 2

After computing the first study (Simulation Procedure 2) the results obtained were:

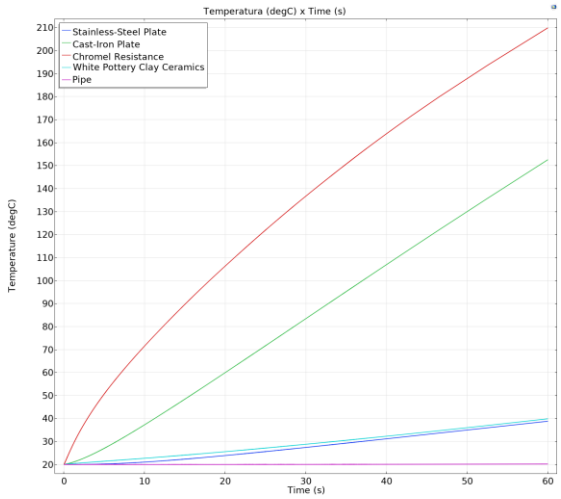

Plot 5 – Simulation 2 - Heating Curve – Temperature (ºC) x Time (s)

Note that the graph presented (Plot 5) does not have the same values as the 3D model since it is a simplified system, and because the heat sources dissipate different energy values. Despite that, the graphs behave similarly when comparing the magnitude difference between the reactor components.

This model also differentiates from the others analyzed due to the presence of the tubulation. The tubulation contains water, which helps to control the overall system temperature. This component was not implemented on the next simulation procedure because it would take high computational costs, and its impact on the final temperature has a low magnitude.

This simulation was crucial to check initial conditions and to verify the boundary definitions that needed to be applied for the model to work so it could, then, be implemented on a more complex structure, such as Simulation Procedure 3.

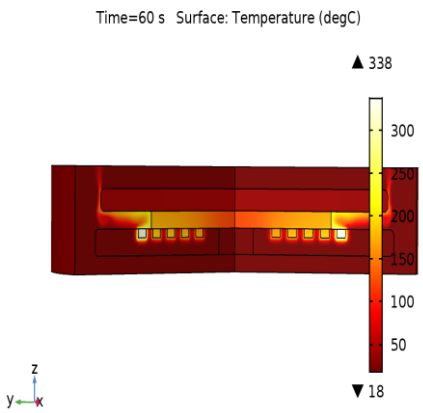

Plot 6 – 3D Plot – Temperature Distribution

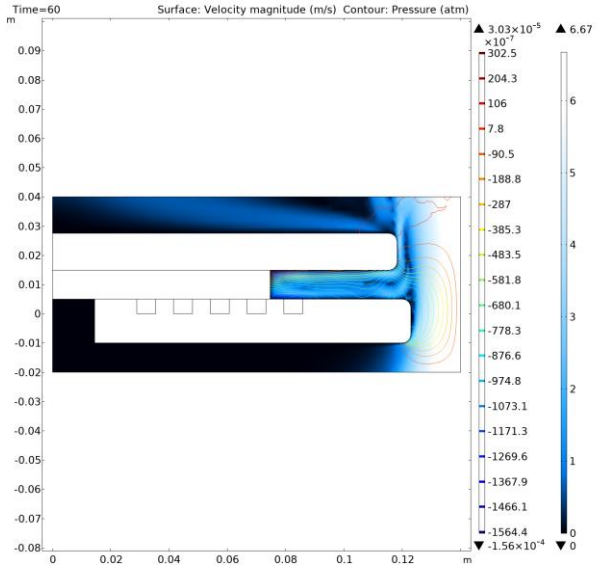

Plot 7 – 2D Plot – Velocity and Pressure

These plots can be visualized as animations, available on YouTube [19], [20], [21].

3.3.Results – Simulation 3

The results obtained after computing Simulation Procedure 3 are stated in Plots 8, 9, 10, and a summary of the final results are compared in Table 10. All the plots are also available as animations [22]. The heat gradient (Plot 9) behaves similarly as seen in Simulation 1 (Plot 4). The main difference, that is discussed in section 3.4, are the final temperature (Plot 8) and the larger time that took for the temperature to stabilize.

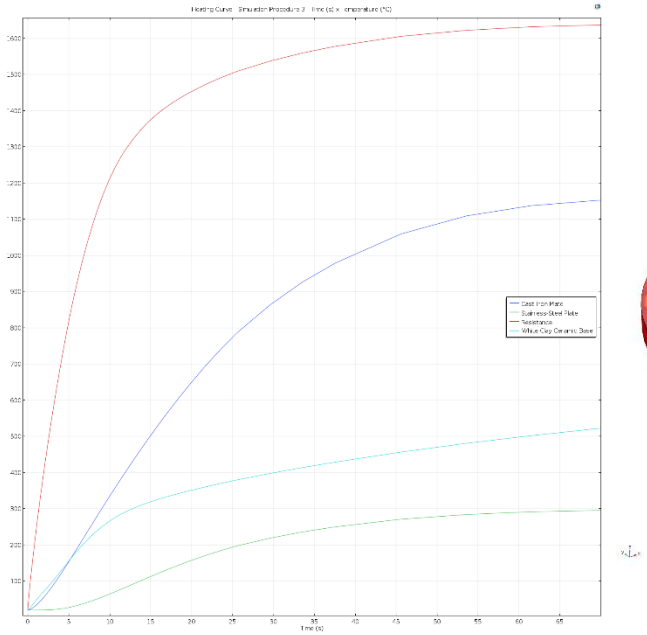

Plot 8 – Simulation 3 – Heating Curve – Temperature (ºC) x Time (s)

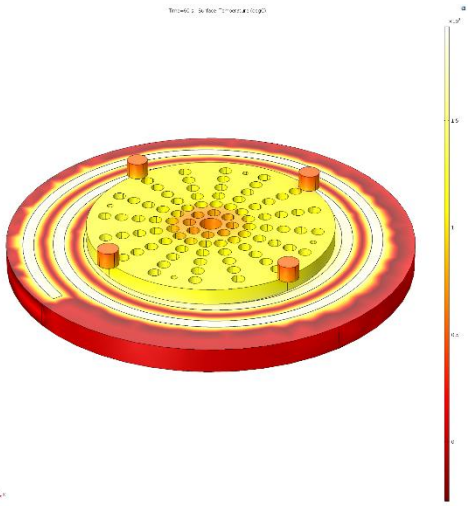

Plot 9 – 3D Plot – Heat Distribution (t = 60 s); (Upper View, Stainless Steel Plate Hidden)

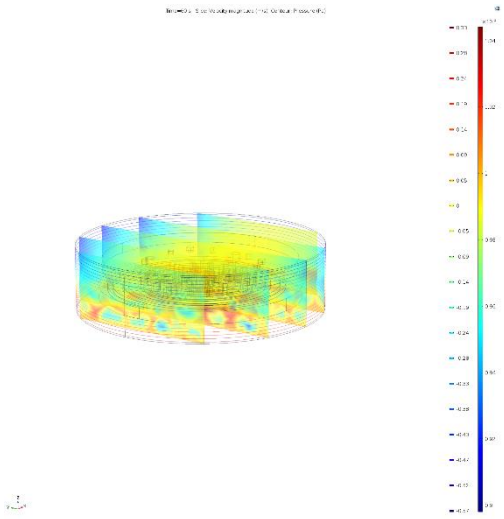

Plot 10 – 3D Plot – Velocity and Pressure (t = 60 s)

3.4. Results Comparative

According to the results obtained (Table 4), with the inclusion of the convection in Simulation Procedure 3, the temperature stabilization time increases. These results agree with the theoretical expectation since the heat exchange with the environment (air) will make the upper plates take a longer time to heat.

Table 4 – Final Temperatures (°C) Comparative

Simulation Procedure 1				
Time (s)	**Cast-Iron (°C)**	**Stainless-Steel (°C)**	**Resistance (°C)**	**Ceramic Base (°C)**
60,714	1163,7	416,1	1640,1	500,27
Simulation Procedure 3				
Time (s)	**Cast-Iron (°C)**	**Stainless-Steel (°C)**	**Resistance (°C)**	**Ceramic Base (°C)**
69,59	1152,2	295,5	1637,1	521,57
Comparative Between Simulation Procedure 1 and 3				
Standard Deviation	8,1	85,3	2,1	15,1
Deviation Mean	27,6			

In Table 4, in which the standard deviation is calculated, after the stabilization period for each version, the highest temperature difference occurs for the stainless-steel plate, which presents a difference of approximately 120 °C between Simulation Procedure 1 and 3. The real reactor has a type of dome that closes its upper part. It serves the purpose of avoiding heat exchange with the environment, and it is also utilized to deposit the product of interest.

Also, we can observe in the temperature comparison chart (Plots 11 and 12) the area between both hatched curves, which is proportional to the heat removed from the system with the addition of this phenomenon. The first hatched area (Plot 11) value is 9.51e+3, and the second area (Plot 12) value is 2.74e+3, both areas were calculated with the data analysis software *QtiPlot*.

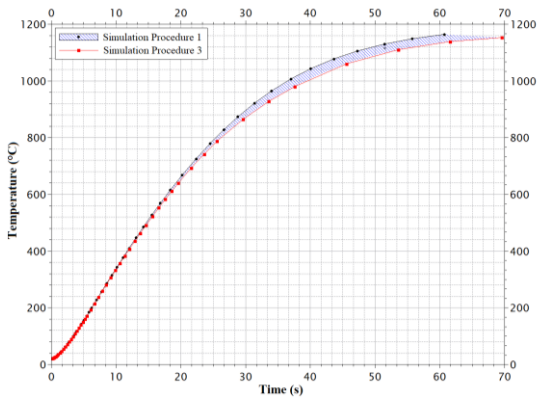

Plot 11 – Temperature Comparative – Cast-Iron Plate

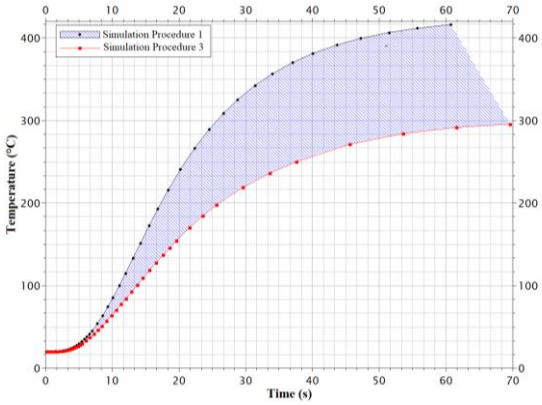

Plot 12 – Temperature Comparative – Stainless-Steel Plate

4. Conclusions

In summary, the simulation results demonstrate that the ALD reactor analyzed has an irregular heat distribution when it reaches the optimum temperature between 300 ˚C and 400 ˚C. The central area of the cast-iron plate is colder mainly because of the component's geometries and positionings, such as the resistance spiral layout (Simulation Procedure 1 and 3) and the positioning of the water tubulation (Simulation Procedure 2) which helps the temperature maintenance and cooling.

In the results section 3.4, it was analyzed how convection is a crucial factor for the heat distribution, and it is also responsible for the heat loss to the environment, especially on the stainless-steel plate, impacting how long it takes for the reactor to stabilize its final temperature during the heating process. For this reason, to avoid heat loss to the environment, the reactor should be more thermally insulated.

To increase the deposition uniformity, we expect that by rotating the reactor plates (cast-iron and stainless-steel plates), the temperature will distribute more evenly. Besides influencing the thermal homogenization, the rotation speed also influences the precursor distribution; in other words, by rotating the reactor, the deposition is more evenly distributed.

Finally, in this study, we developed an ALD reactor model that provides, through simulation, extensive real-time quantitative data about the reactor conditions and facilitates an experimental investigation.

5. Acknowledgments

We thank the financial support obtained from CNPq (National Council for Scientific and Technological Development) during the period of elaboration of this work.

6. References

All images corresponding to 2D, 3D models and plots were exported from the software COMSOL Multiphysics interfaces using prints or the capture function.

[1] S. M. George, "Atomic Layer Deposition: An Overview," no. 110 (1), 111-131, 2009.

[2] Ultratech, "Atomic Layer Deposition - Ultratech/CNT," 2016. [Online]. Available: http://www.cambridgenanotechald.com/atomic-layer-deposition/index.shtml. [Accessed 15 April 2017].

[3] R. W. Johnson, A. Hultqvist and S. F. Bent, "A brief review of atomic layer deposition: from fundamentals to applications," vol. 17, no. 5, 2014.

[4] A. Pakkala and M. Putkonen, Handbook of Deposition Technologies for Films and Coatings, Third Edition ed., P. M. Martin, Ed., William Andrew Publishing, 2010, pp. 364 - 391.

[5] D. Hausmann, "How Atomic Layer Deposition Works," 15 March 2018. [Online]. Available: https://semiengineering.com/a-look-at-atomic-layer-deposition-2/. [Accessed 05 August 2020].

[6] ASM International, "Atomic Layer Deposition," [Online]. Available: https://www.asm.com/technology/key-technologies/atomic-layer-deposition. [Accessed 05 August 2020].

[7] Scientific Rana, "COMSOL: (I/II) Complex 3D Geometry construction using Basic Mathematics L-7," 25 September 2016. [Online]. Available: https://youtu.be/54Hwtv2Zkqs. [Accessed 25 July 2020].

[8] Scientific Rana, "COMSOL: (II/II) Complex 3D Geometry construction using Basic Mathematics L-7," 25 September 2016. [Online]. Available: https://youtu.be/5435CUmznLI. [Accessed 25 July 2020].

[9] K. Vyshenska, "How to Build a Parameterized Archimedean Spiral Geometry," 27 July 2016. [Online]. Available: https://br.comsol.com/blogs/how-to-build-a-parameterized-archimedean-spiral-geometry. [Accessed 27 July 2020].

[10] COMSOL, "Form Union and Form Assembly in COMSOL Multiphysics Explained," 10 March 2015. [Online]. Available: https://www.youtube.com/watch?v=Q7fOawr58H0. [Accessed 26 July 2020].

[11] COMSOL, "Heat Transfer Module User's Guide," 2018. [Online]. Available: https://doc.comsol.com/5.4/doc/com.comsol.help.heat/HeatTransferModuleUsersGuide.pdf. [Accessed 5 August 2020].

[12] COMSOL, "AC/DC Module User's Guide," 2017. [Online]. Available: https://doc.comsol.com/5.3/doc/com.comsol.help.acdc/ACDCModuleUsersGuide.pdf. [Accessed 5 August 2020].

[13] COMSOL, "Simulating Feedback Control of Thermal Systems," 2015. [Online]. Available: https://br.comsol.com/video/simulating-feedback-control-thermal-systems. [Accessed 26 July 2020].

[14] COMSOL, "COMSOL Multiphysics Reference Manual," 2019. [Online]. Available: https://doc.comsol.com/5.5/doc/com.comsol.help.comsol/COMSOL_ReferenceManual.pdf. [Accessed 5 August 2020].

[15] COMSOL, "CFD Module Users Guide," 2018. [Online]. Available: https://doc.comsol.com/5.4/doc/com.comsol.help.cfd/CFDModuleUsersGuide.pdf. [Accessed 05 August 2020].

[16] W. Frei, "Modeling Natural and Forced Convection in COMSOL Multiphysics®," 28 April 2017. [Online]. Available: https://br.comsol.com/blogs/modeling-natural-and-forced-convection-in-comsol-multiphysics/. [Accessed 01 August 2020].

[17] COMSOL, "Using Plots to Visualize Results in COMSOL Multiphysics®," [Online]. Available: https://br.comsol.com/video/plots-visualize-results-comsol-multiphysics. [Accessed 27 July 2020].

[18] A. B. Suppelsa, "COMSOL - Simulation Procedure 1 - Heat Distribution Lateral View 3D Plot," 21 August 2020. [Online]. Available: https://www.youtube.com/watch?v=avEBoOptdYo.

[19] A. B. Suppelsa, "COMSOL - Simulation Procedure 2 - Isothermal Contour Plot," 19 August 2020. [Online]. Available: https://www.youtube.com/watch?v=RgHnthzm0QM.

[20] A. B. Suppelsa, "COMSOL - Simulation Procedure 2 - Velocity and Pressure Plot," 20 August 2020. [Online]. Available: https://www.youtube.com/watch?v=a_wwoETqEGo.

[21] A. B. Suppelsa, "COMSOL - Simulation Procedure 2 - Heat Distribution 3D Plot," 19 August 2020. [Online]. Available: https://www.youtube.com/watch?v=W_JB7llZWw4.

[22] A. B. Suppelsa, "COMSOL - Simulation Procedure 3 - Heat Distribution 3D Plot," 19 August 2020. [Online]. Available: https://www.youtube.com/watch?v=5E2Vae-MsFk.

[23] Engineering ToolBox, "Metals and Alloys - Densities," 2004. [Online]. Available: https://www.engineeringtoolbox.com/metal-alloys-densities-d_50.html. [Accessed 26 July 2020].

[24] John Wiley & Sons, Inc., "APPENDIX A: Thermophysical Properties - Fundamentals of Heat Exchanger Design," 2003. [Online]. Available: https://onlinelibrary.wiley.com/doi/pdf/10.1002/9780470172605.app1. [Accessed 26 July 2020].

[25] Engineers Edge, "Thermal Properties of Metals, Conductivity, Thermal Expansion, Specific Heat," [Online]. Available: https://www.engineersedge.com/properties_of_metals.htm. [Accessed 26 July 2020].

[26] Engineering ToolBox, "Emissivity Coefficients Materials," 2003. [Online]. Available: https://www.engineeringtoolbox.com/emissivity-coefficients-d_447.html. [Accessed 26 July 2020].

[27] Engineers Edge, "Specific Heat Capacity of Metals Table Chart," [Online]. Available: https://www.engineersedge.com/materials/specific_heat_capacity_of_metals_13259.htm. [Accessed 26 July 2020].

[28] Optotherm, Inc., "Emissivity Table," [Online]. Available: https://www.optotherm.com/emiss-table.htm. [Accessed 26 July 2020].

[29] Concept Alloys, Inc, "Electrical Resistance Nickel-Chromium 80-20 Chromel® A Wire," [Online]. Available: https://conceptalloys.com/concept-alloys-intellectual-property/. [Accessed 26 July 2020].

[30] W. Frei, "Using Virtual Operations to Simplify Your Geometry," 28 November 2014. [Online]. Available: https://br.comsol.com/blogs/using-virtual-operations-simplify-geometry/. [Accessed 27 July 2020].

[31] C. Fairclough, "Efficiently Mesh Your Model Geometry with Meshing Sequences," 18 August 2016. [Online]. Available: https://br.comsol.com/blogs/efficiently-mesh-your-model-geometry-with-meshing-sequences/. [Accessed 26 July 2020].

[32] COMSOL, "Material Properties On A Boundary," 15 August 2011. [Online]. Available: https://br.comsol.com/forum/thread/21640/material-properties-on-a-boundary. [Accessed 2020 July 26].